Development 127, 679-691 (2000)
Printed in Great Britain © The Company of Biologists Limited 2000
DEV8687

Organ shape in the *Drosophila* salivary gland is controlled by regulated, sequential internalization of the primordia

Monn Monn Myat and Deborah J. Andrew*

Department of Cell Biology and Anatomy, The Johns Hopkins University, School of Medicine, 725 N. Wolfe Street, Baltimore, MD 21205-2196, USA
*Author for correspondence (e-mail: dandrew@jhmi.edu)

Accepted 22 November 1999; published on WWW 26 January 2000

SUMMARY

During *Drosophila* development, the salivary primordia are internalized to form the salivary gland tubes. By analyzing immuno-stained histological sections and scanning electron micrographs of multiple stages of salivary gland development, we show that internalization occurs in a defined series of steps, involves coordinated cell shape changes and begins with the dorsal-posterior cells of the primordia. The ordered pattern of internalization is critical for the final shape of the salivary gland. In embryos mutant for *hückebein* (*hkb*), which encodes a transcription factor, or *faint sausage* (*fas*), which encodes a cell adhesion molecule, internalization begins in the center of the primordia, and completely aberrant tubes are formed. The sequential expression of *hkb* in selected cells of the primordia presages the sequence of cell movements. We propose that *hkb* dictates the initial site of internalization, the order in which invagination progresses and, consequently, the final shape of the organ. We propose that *fas* is required for *hkb*-dependent signaling events that coordinate internalization.

Key words: *Drosophila, faint sausage, folded gastrulation, hückebein*, Invagination, Morphogenesis, Salivary gland

INTRODUCTION

During embryonic development, morphogenetic movements form the three germ layers and give shape to tissues and organs specific to each organism. Despite the wide variety in the shapes of epithelial tissues and organs that form within and among different organisms, only three morphogenetic mechanisms have been described for creating them. Epithelial invagination is the most prevalent mechanism, and is observed during formation of the avian lens and optic cup (Hilfer, 1983), the avian otic vesicle (Alvarez and Navascues, 1990), the avian and mammalian neural tube (reviewed in Schoenwolf and Smith, 1990), and *Drosophila* and *Xenopus* gastrulations (Hardin and Keller, 1988; reviewed in Leptin, 1999). During this process, cells of the epithelial sheet change shape from columnar to wedge-shaped by constriction of the apical surface membrane and basal migration of nuclei. This cellular shape change results in the inward folding of the epithelial sheet and formation of a pit (Ettensohn et al., 1985; Gumbiner, 1992). In the second mechanism, directed cell migration in the presence or absence of cell proliferation forms branching tubular organs, such as the mammalian lung and *Drosophila* trachea (reviewed in Hogan and Yingling, 1998; Metzger and Krasnow, 1999). The third mechanism involves cell condensation followed by the formation of a central lumen. Mammalian kidney tubules are formed by this mechanism (for a review see Davies and Bard, 1998).

Since the early 1900s, histological studies have revealed the frequent occurrence of epithelial invaginations during embryonic development (Minot, 1903), and have led to speculations concerning the mechanisms driving this process (Gudernatsch, 1913; Glaser, 1916). However, it is only in the last two decades that molecules controlling epithelial morphogenesis have been discovered. In vitro tissue and organ culture studies identified scatter factor/hepatocyte growth factor (SF/HGF) as a morphogen that induces mammalian cells, such as Madin-Darby canine kidney (MDCK) cells, to form tube-like structures when grown in collagen gels (Montesano et al., 1991a,b; Bowes et al., 1999). SF/HGF acts in a paracrine and/or autocrine manner to induce the mesenchymal-epithelial transition that occurs during kidney development, and to induce branching of the ureteric bud (Woolf et al., 1995). In addition to SF/HGF, other secreted growth factors, such as EGF, TGF-α, TGF-β and FGFs, have been shown to either induce or inhibit tube formation (Kjelsberg et al., 1997; Sakurai and Nigam, 1997; Sakurai, H. et al., 1997; Sakurai, Y. et al., 1997; Vainio and Muller, 1997).

Genetic studies in *Drosophila* have also identified several molecular components controlling epithelial morphogenesis. During early *Drosophila* gastrulation, the mesodermal and endodermal primordia are internalized by an invagination event involving cell shape changes (Leptin and Grunewald, 1990; Sweeton et al., 1991). Two signaling molecules are known to regulate this process: *folded gastrulation* (*fog*) and *concertina* (*cta*). *fog* encodes a putative secreted molecule that signals via an unknown receptor to *cta*, which encodes a putative Gα-like

protein, which then relays the signal to the cytoskeleton to promote cell shape change (Parks and Wieschaus, 1991; Costa et al., 1994). In embryos mutant for either *fog* or *cta*, apical constrictions either do not occur at all, as in endodermal primordial invagination, or do not occur in a coordinated manner, as in mesodermal primordial invagination (Costa et al., 1994). One possible mechanism by which the *fog/cta* pathway could regulate the cytoskeleton is through *RhoGEF2* (Barrett et al., 1997). Rho GTPases, such as RhoGEF2, are key regulators of cytoskeletal rearrangement in mammalian cells (Ridley, 1995), and also play an essential role in *Drosophila* gastrulation. *Drosophila* embryos lacking *RhoGEF2* display defects in mesodermal and endodermal primordial invaginations that are similar to those of *fog* and *cta* mutant embryos (Barrett et al., 1997; Hacker and Perrimon, 1998).

Studies in the *Drosophila* trachea have identified several key components required for internalization and migration of tracheal precursors. The tracheal system originates from 20 ectodermal placodes that invaginate and then migrate and fuse to form an elaborate network of branches that provide oxygen to all internal tissues (Campos-Ortega and Hartenstein, 1997). While the transcription factor, *trachealess* (*trh*) (Isaac and Andrew, 1996; Wilk et al., 1996), and EGF-signaling (Llimargas and Casanova, 1999) are required for invagination of the tracheal placodes, members of the FGF-signaling pathway, such as *breathless* and *branchless* are required for branching of the tracheal tubes (Glazer and Shilo, 1991; Sutherland et al., 1996). In contrast to the general requirement for the FGF-pathway in tracheal branching, the DPP- and EGF-signaling pathways are required for the migration of only certain branches of the trachea (Vincent et al., 1997; Wappner et al., 1997).

Constructing the final shape of an organ is undoubtedly a complex developmental process where multiple levels of regulation have to be coordinated spatially and temporally. Several questions remain unanswered regarding organ formation. (1) What early signaling events select the correct site within the primordial field for the initial cell shape changes? (2) How are cell shape changes coordinated spatially and temporally? (3) Once cells have been internalized, how are they guided into the interior of the embryo? (4) How is the final shape of the organ achieved and maintained? The *Drosophila* salivary gland is an excellent model system for investigating both the genetics and cell biology of organ development. It is a simple tubular organ composed of only two cell types, the secretory cells, which synthesize and secrete proteins, and the duct cells, which form the tubes connecting the secretory cells to the larval mouth (for a review, see Andrew et al., in press). The salivary gland primordia arise from two ventral ectodermal placodes in the region of the presumptive posterior head (Campos-Ortega and Hartenstein, 1997). Once the primordia are established, the cell number is fixed, with no additional cell divisions or programmed cell deaths, which greatly simplifies morphogenetic studies of salivary gland development.

In this report, we demonstrate that invagination of the *Drosophila* salivary glands is initiated in a specific group of primordial cells, and continues in a regulated, sequential order. We propose that the selection of the correct site of invagination, and the order in which cells invaginate, determine the final shape of the salivary glands. Abrogation of these two early events, such as in embryos mutant for either *huckebein* (*hkb*), a predicted zinc finger transcription factor (Brönner et al., 1994), or *faint sausage* (*fas*), an immunoglobulin-like cell adhesion molecule (Lekven et al., 1998), results in salivary glands whose final shape is significantly altered.

MATERIALS AND METHODS

Fly stocks

The wild-type flies used in all experiments were Oregon R. hkb^{A231R}, hkb^{2}, fas^{I} and fas^{II} alleles are described in Flybase (1999).

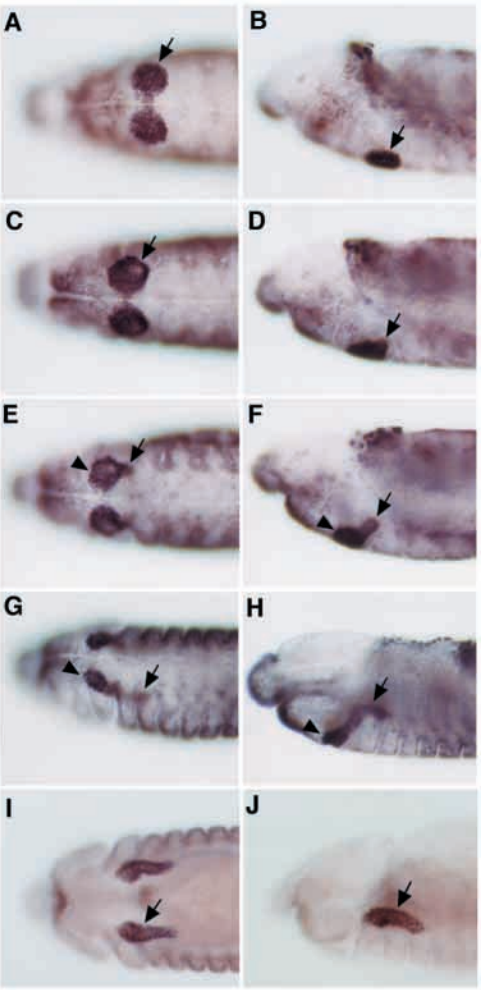

Fig. 1. Salivary gland internalization in wild-type embryos occurs in four stages. Embryos in (A-F) are at embryonic stage 11, the embryo in (G,H) is at stage 12, and the embryo in (I,J) is at embryonic stage 14. (A,C,E,G, I) Ventral views; (B,D,F,H,J) the corresponding lateral views. Salivary gland placode cells marked with dCREB-A staining are found at the ventral surface (A,B, arrows; stage I). The dorsal-posterior cells of the placode invaginate first to form a pit (C,D, arrows; stage II). A narrow salivary gland tube (E,F, arrows) forms at the posterior end of the placode, while the remainder of the gland appears bulbous (E,F, arrowhead, stage III). As more cells internalize, the salivary gland tube lengthens (G,H, stage IV). The distal portion of the gland is directed posteriorly (G,H, arrowhead) and the proximal portion of the gland is directed approximately dorsally (H, arrow). After internalization of the secretory cells is complete, the salivary glands appear as two elongated tubular structures (I,J, arrows).

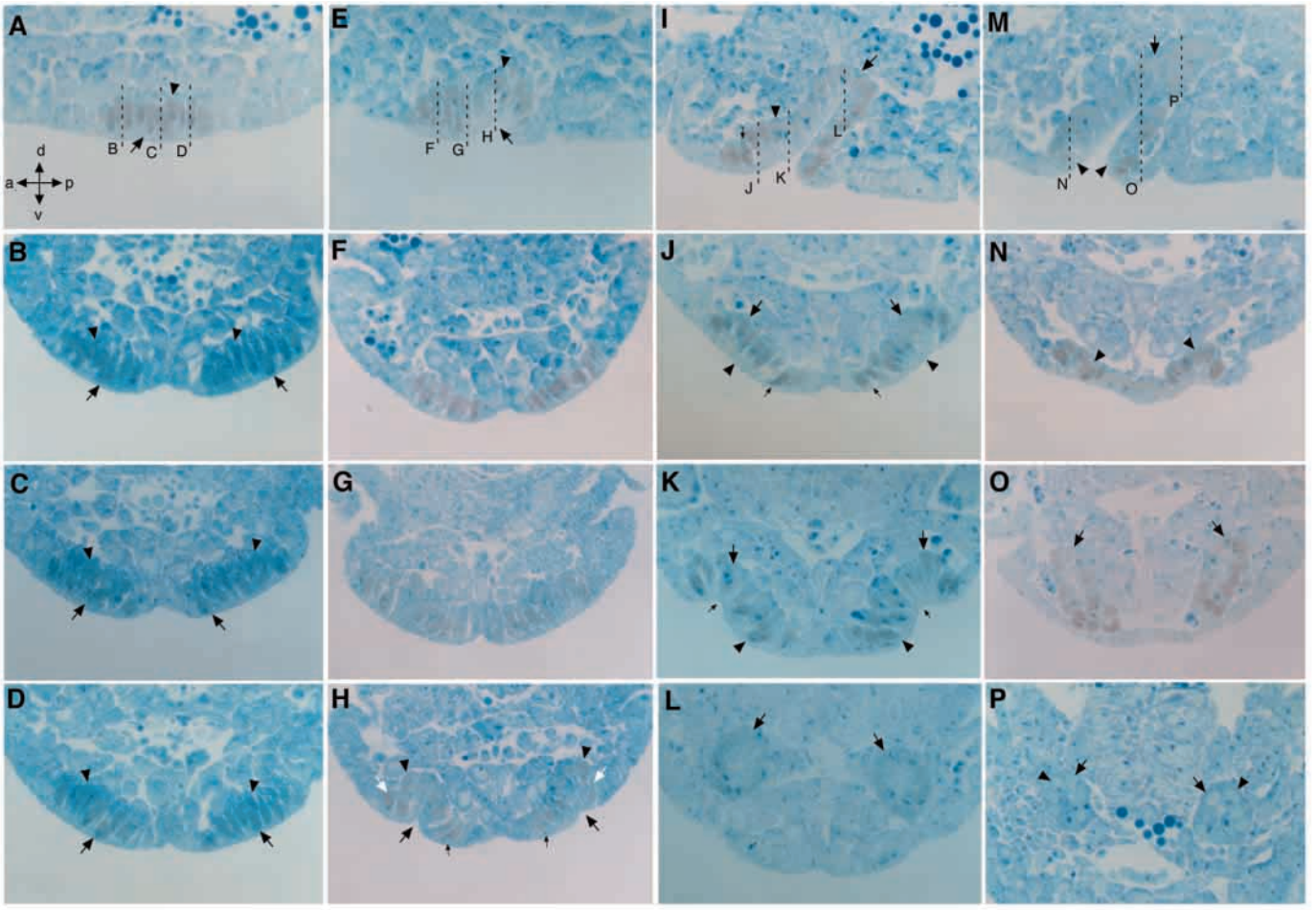

Fig. 2. Histological analysis of salivary gland internalization in wild-type (WT) embryos. (A,E,I,M) Transverse sections of WT embryos at stages I, II, III and IV, respectively, of salivary gland internalization. For each transverse section represented in the top row, there are three cross sections in the three panels below representing the anterior, medial and posterior regions. These regions are indicated by letters and dashed lines in the transverse sections. Cells of the salivary gland placode at stage I are elongated, with their nuclei randomly located in the apical (A-D, arrows) and basal domains (A-D, arrowheads). In stage II (E-H), the invaginating dorsal-posterior cells (E,H) are wedge-shaped with constricted apices (arrows), and basal nuclei (arrowheads), while the ventral-posterior cells (H) remain elongated with broad, unconstricted apices and nuclei in random positions (H, small arrows), like the cells in the anterior (F) and medial (G) regions of the placode. Cells at the dorsal-posterior edge of the invaginating pit are elongated with unconstricted apices and nuclei in random positions (H, white arrows). In stage III (I-L), a salivary gland tube is formed at the posterior end of the placode (I,L, arrows). Cells in the dorsal-medial (K) region of the placode are wedge-shaped with constricted apices (small arrow), and basal nuclei (large arrow), while the ventral-medial cells are elongated with unconstricted apices and nuclei in random positions (K, arrowheads). In the dorsal-anterior cells (J), nuclei are found basally (large arrow), although the apical surfaces are unconstricted (arrowhead). The ventral-anterior cells are elongated with unconstricted apices and nuclei in random positions (J, small arrows). In stage IV (M-P), most of the cells of the salivary gland placode have invaginated (M,O,P, arrows), and the internalized salivary gland is an elongated tube (M,P, arrows). Cells within the salivary gland tube retain their wedge-shaped morphology (P, arrowheads). The ring of cells at the ventral surface is in the process of being internalized (M,N, arrowheads). A minimum of three embryos for each view and at each stage of invagination was analyzed. Although only three representative cross sections are shown, 1 μm thin sections of the entire salivary gland primordia at the indicated stages of invagination were acquired for analysis.

Antibody staining and whole-mount in situ hybridizations

The dCREB-A antibody was prepared by K. D. Henderson as described (Andrew et al., 1997), and the rat anti-FAS antibody was a kind gift of V. Hartenstein. The mouse monoclonal β-gal antibody was obtained from Promega Corp. (Madison, WI, USA). Embryo fixation and staining were performed as described (Reuter et al., 1990). Mutant embryos, homozygous for the *hkb* and *fas* alleles, were distinguished from their heterozygous siblings by the absence of staining for β-gal, which marks the *Ubx-lacZ* insert on the TM6B balancer chromosome and the *ftz-lacZ* insert on the CyO balancer chromosome of non-mutant embryos. Immunostained embryos and embryos processed for whole-mount in situ hybridizations were visualized and photographed on a Zeiss Axiophot microscope (Carl Zeiss, Thornwood, NY, USA) using Nomarski optics and Kodak print film (Eastman Kodak, Rochester, NY, USA). Embryonic mRNA was detected by whole-mount in situ hybridization as described by Lehmann and Tautz (1994). Embryos were mounted in 70% glycerol and visualized and photographed as for antibody staining.

Thick sections of epon-embedded embryos

Embryos were processed for antibody staining with α-dCREB-A and α-β-gal as described above. After dehydration in an ethanol series, embryos were infiltrated with propylene oxide (Polysciences Inc, Warrington, PA, USA) as the transitional solvent. Embryos were

embedded in a gradual series of propylene oxide and an epoxy resin (Eponate Kit™, Ted Pella, Reading, CA, USA). After aligning the embryos for either cross or sagittal sections, embryos were baked overnight at 60°C. 1 μm thick sections were cut with a glass knife (Leica Inc, Deerfield, IL) on a Reichart-Jung Ultracut E (Leica Inc.). Sections were transferred to glass slides (Fisher Scientific, Pittsburgh, PA) and counterstained with 1% Methylene Blue and 1% sodium borate (Sigma, Missouri, IL). Stained sections were mounted in Permount (Fisher Scientific), and viewed and photographed as described above for antibody-stained embryos.

Scanning electron microscopy

Embryos were collected and dechorionated as described above for antibody staining. Embryos were then fixed at the interface of heptane (Sigma) and a mixture of 3.7% formaldehyde (Fisher Scientific) and 0.5% glutaraldehyde (Polysciences Inc.) for 15 minutes. After removal of the vitelline membrane by methanol washes, antibody staining for β-Gal was performed as described above to distinguish unambiguously homozygous mutant embryos from their heterozygous siblings. The selected homozygous mutant embryos were then refixed in 12.5% glutaraldehyde (Ted Pella) for 2 hours. After a post-fixation in 1% osmium tetroxide (Polysciences Inc.) in 0.1 M cacodylate buffer (Polysciences Inc.), embryos were dehydrated in an ethanol series, and dried in Peldri (Ted Pella). Processed embryos were adhered to aluminum mounts (Structure Probe Inc, West Chester, PA, USA) using carbon conductive tabs (Ted Pella). After coating with gold palladium on a Denton Vacuum sputter coater (Moorestown, NJ, USA), embryos were viewed on an Amray 1810 scanning electron microscope (Bedford, MA, USA), and photographed using Type 55 Polaroid film (Polaroid Corp., Cambridge, MA, USA).

RESULTS

Salivary glands are internalized through apical constriction

During embryogenesis, cells of the salivary gland primordia, which initially reside at the ventral surface, are internalized to form the tubular salivary glands in less than 4 hours. To analyze gross morphology during internalization, we stained wild-type (WT) embryos with antisera to dCREB-A, a transcription factor expressed to high levels in the nuclei of salivary gland secretory cells (Smolik et al., 1992; Andrew et al., 1997), and examined whole-mount embryos. From this analysis, we can describe four distinct stages of salivary gland internalization. During stage I, the salivary gland secretory cell primordia forms the two salivary gland placodes at the ventral surface of the embryo (Fig. 1A,B). During stage II, an invaginating pit forms in the dorsal-posterior region of each placode, about one to two rows of cells from the dorsal-posterior edge (Fig. 1C,D). During stage III, a non-uniform tube is observed with a narrow distal portion, which forms from the dorsal-posterior cells that internalized first, and a bulbous proximal portion, which forms when both dorsal-medial and dorsal-anterior cells are internalized (Fig. 1E,F). As the remaining ventral cells of the placode invaginate during stage IV, a more uniformly sized, bent tubular organ is formed (Fig. 1G,H). The distal portion of the tube is directed posteriorly and the proximal portion of the tube is directed approximately dorsally (Fig. 1H). Salivary gland secretory cell internalization is complete when the last ring of cells invaginates. Once the duct cells have internalized, the secretory portion of the gland is ‘cigar-shaped’, and is directed posteriorly, extending to the level of the third thoracic segment and dorsolateral to the ventral nerve cord (Fig. 1I,J).

We performed histological analyses of salivary glands at the four stages described above to analyze changes in cell shape during internalization (Fig. 2). During stage I, when the salivary gland placode cells are at the ventral surface, they are elongated, and their nuclei are distributed randomly between the apical and basal portions of the cells, and cell morphology is uniform throughout the primordia (Fig. 2A-D). During stage II, cells in the dorsal-posterior region of the placode are wedge-shaped and have invaginated to form a small pit. The apical surface membranes of the dorsal-posterior cells are constricted and their nuclei are uniformly localized to a basal domain within each cell (Fig. 2E,H). In contrast, 2-3 rows of cells at the ventral-posterior edge of each primordia (Fig. 2H), and the remainder of cells in the placode (Fig. 2E-H) do not change shape and appear as they did in stage I. One or two rows of cells at the dorsal-posterior edge of the primordia also remain anchored at the ventral surface, with no change in cell shape, apical membrane surface area or nuclear position (Fig. 2H). Sections through the salivary glands at stage III reveal a tube made up of a single layer of wedge-shaped cells surrounding a central lumen (Fig. 2I-L). During this stage, dorsal-medial cells have a characteristic wedge-shaped morphology with constricted apices and basal nuclei (Fig. 2K). The dorsal-anterior cells are becoming wedge-shaped; their nuclei have migrated basally, but their apical membrane is unconstricted (Fig. 2J). The ventralmost 2-3 rows of cells have not undergone any cell shape changes (Fig. 2J,K), and remain elongated with randomly located nuclei, like all placode cells at stage I. During stage IV of internalization, most of the secretory cells have invaginated into an elongated tube (Fig. 2M,O,P), with only a ring of cells remaining at the ventral surface (Fig. 2M,N). When this last ring of cells invaginates by changing shape, internalization of the secretory cells is complete. Although cells of the salivary gland tube remain wedge-shaped, they appear shorter then when they were at the embryo surface (compare Fig. 2P with H,K), suggesting that additional cell shape changes occur once cells are internalized. We conclude that salivary gland internalization occurs through a wave of cell shape changes that begins with the dorsal-posterior cells. As dorsal-medial cells change shape and invaginate to follow the ingressing dorsal-posterior cells, the dorsal-anterior cells begin to change shape and invaginate. Next, the ventral-anterior and then the ventral-posterior cells change shape and invaginate. The last secretory cells to invaginate and internalize include the cells originally located at the dorsal-posterior edge of the placode. These data show that salivary gland internalization occurs, at least in part, through a mechanism driven by cell shape change, and suggest that the migration of nuclei to the basal domain and subsequent constriction of the apical surface membrane are prerequisites for cell shape change and invagination. These studies do not rule out the existence of additional forces driving internalization of this tissue.

Scanning electron microscopy reveals changes in surface morphology during salivary gland internalization

The wave of apical constrictions that accompany the cell shape changes observed using histological techniques was also observed by scanning electron microscopy (SEM) analysis of

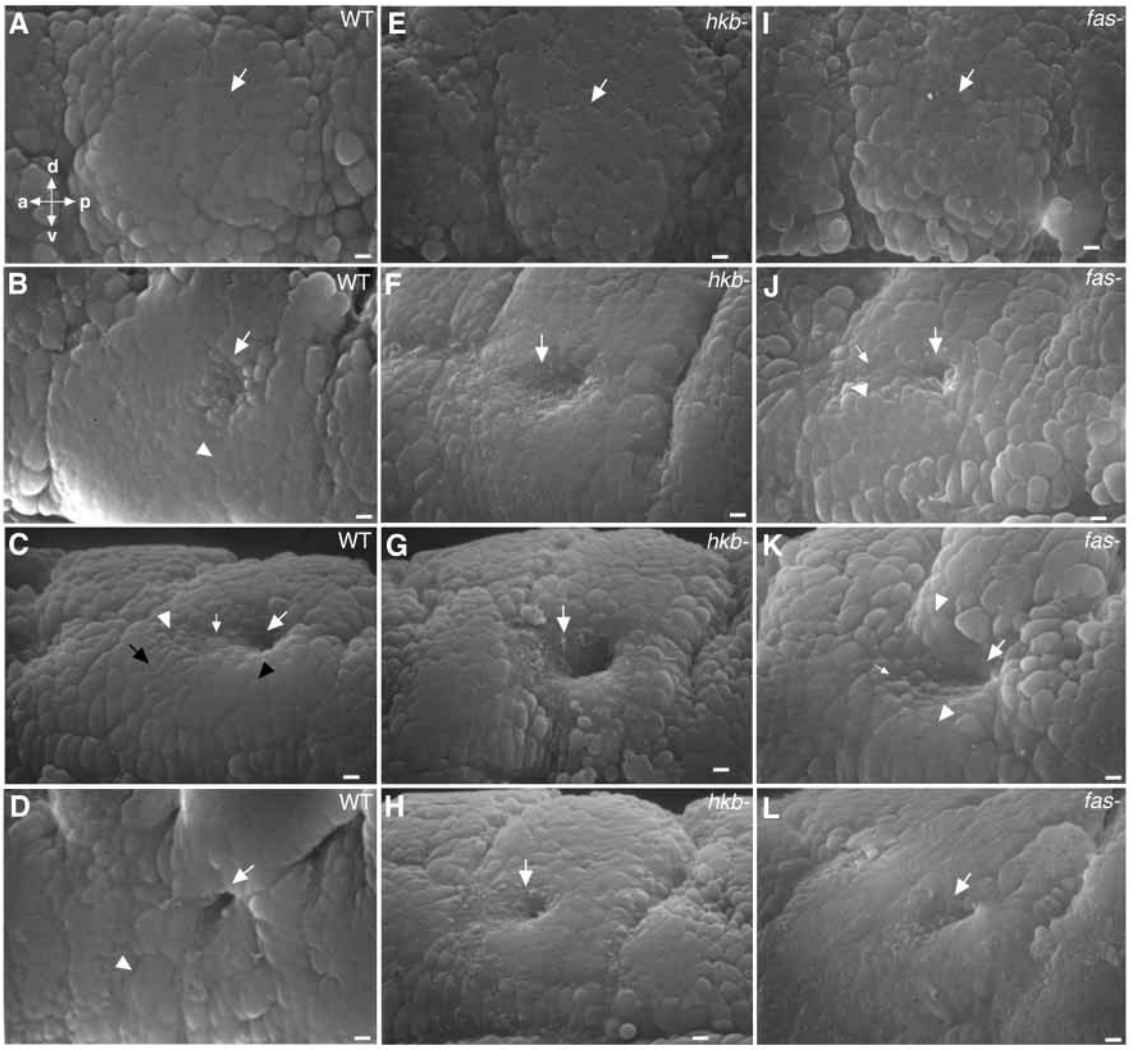

Fig. 3. Surface morphology of the invaginating salivary glands in wild-type (WT) embryos, and *hkb* and *fas* mutant embryos. SEM images of WT embryos (A-D), *hkb* mutant embryos (E-H) and *fas* mutant embryos (I-L). In (A) the arrow points to the broad, flat surface of salivary gland placode cells. Invaginating dorsal-posterior cells have round apices (B, arrow) compared to those of neighboring placode cells (B, arrowhead). The stream of cells migrating into the invaginating pit (C, large white arrow), have apical membrane protrusions (C, small white arrow), round apical surfaces (C, white arrowhead) and narrowed, but flat apical surfaces (C, black arrow). Cells ventral-posterior to the invaginating pit have broad, flat apical surfaces (C, black arrowhead). The salivary gland pit after completion of invagination (D, arrow) is surrounded by cells with broad apical surfaces (D, arrowhead). In (E) the arrow points to the broad, flat surface of *hkb* salivary gland placode cells. Invagination is initiated in the center of the placode (F, arrow). Cells immediately surrounding the pit invaginate (G, arrow). The remaining pit, after invagination is complete (H, arrow), is similar to that in WT embryos (D). In (I) the arrow points to the broad, flat surface of *fas* salivary gland placode cells. Invagination begins in the center of the placode (J, large arrow). Cells immediately anterior to the pit have apical membrane protrusions (J, small arrow) and round (J, arrowhead) apices. The invaginating pit lengthens anteriorly (K, arrow) with cells immediately anterior having round apices (K, small arrow) while cells in the remainder of the placode have broad and flat apices (K, arrowheads). The remaining pit after invagination is complete (L, arrow) is similar to the pits of WT (D) and *hkb* (H) mutant embryos. D, dorsal; V, ventral; A, anterior; P, posterior. A minimum of five WT, *hkb* and *fas* embryos at each stage of invagination was analyzed. Bar, 2.5 μm.

the surface morphology of invaginating secretory cells. Prior to any invagination event, the surface of the salivary gland placode has a flattened appearance compared to the round surfaces of neighboring non-salivary gland cells (Fig. 3A). The first cell shape changes are observed in the dorsal-posterior region of the placode, where the apical surfaces of the cells appear rounder and narrower, compared to the broad, flat surfaces of neighboring salivary gland cells (Fig. 3B). As invagination progresses, the changes in the surface morphology of cells in different regions of the salivary gland primordia reflects the order in which they will be internalized (Fig. 3C). The cells immediately anterior to the pit, which is still located in a dorsal-posterior position, display numerous membrane ruffles at their apical surface. These are the cells that will invaginate next. Cells that are slightly more anterior, the dorsal-anterior cells, have constricted their apical surface membranes, and their apices are round. The apices of the ventral-anterior cells, which will invaginate after the dorsal-anterior cells, are narrower than at earlier stages but are not round. Finally, the apical surfaces of the ventral-posterior cells, which are among the last to internalize, remain flat and broad. Once internalization of the secretory cells is complete, an open pit

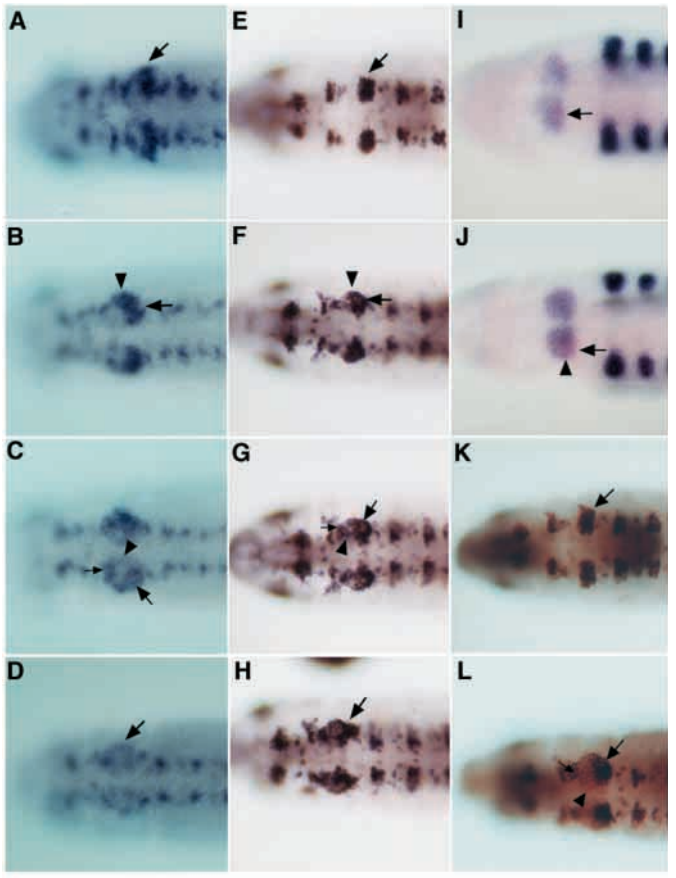

Fig. 4. *hkb* is expressed in a dynamic pattern in the salivary gland placode. (A-D) Whole-mount in situ hybridizations of WT embryos using an antisense *hkb* RNA probe. (E-H) Embryos with the AI7-*hkb* P-element insert stained for β-gal. (I,J) Whole-mount in situ hybridizations of WT embryos double labeled for *hkb* (red) and *trh* (blue). (K,L) AI7-*hkb* embryos double labeled with α-β-gal (dark brown) to detect *hkb* expression and α-dCREB-A (light brown) to mark the entire salivary placode. *hkb* RNA and β-gal are first detected in the posteriormost region of the salivary placode (A,E,I,K. arrows). *hkb* expression expands to include the dorsal-posterior cells and the dorsal-medial cells (B,F,J, arrows and arrowheads, respectively). *hkb* is detected in the dorsal-posterior cells (C,G,L, large arrows) and in the dorsal-anterior cells (C,G,L, small arrows), but is only faintly detected in the ventral region of the placode (C,G,L, arrowheads). *hkb* RNA levels then gradually decrease in the salivary placode (D, arrow), while β-gal continues to be expressed (H, arrow).

remains, which is surrounded by the broad round surfaces of neighboring cells (Fig. 3D). Thus, based on our SEM data and our examination of histological sections of salivary glands at multiple stages, we conclude that internalization of the secretory cells in WT embryos occurs through a wave of regulated, sequential invagination events.

hkb is expressed in a dynamic pattern in the early salivary gland

Among the earliest genes expressed in the salivary glands is *hückebein* (*hkb*), which encodes an Sp1/egr-like transcription factor (Brönner et al., 1994). Whole-mount in situ hybridization to detect *hkb* RNA in WT embryos and

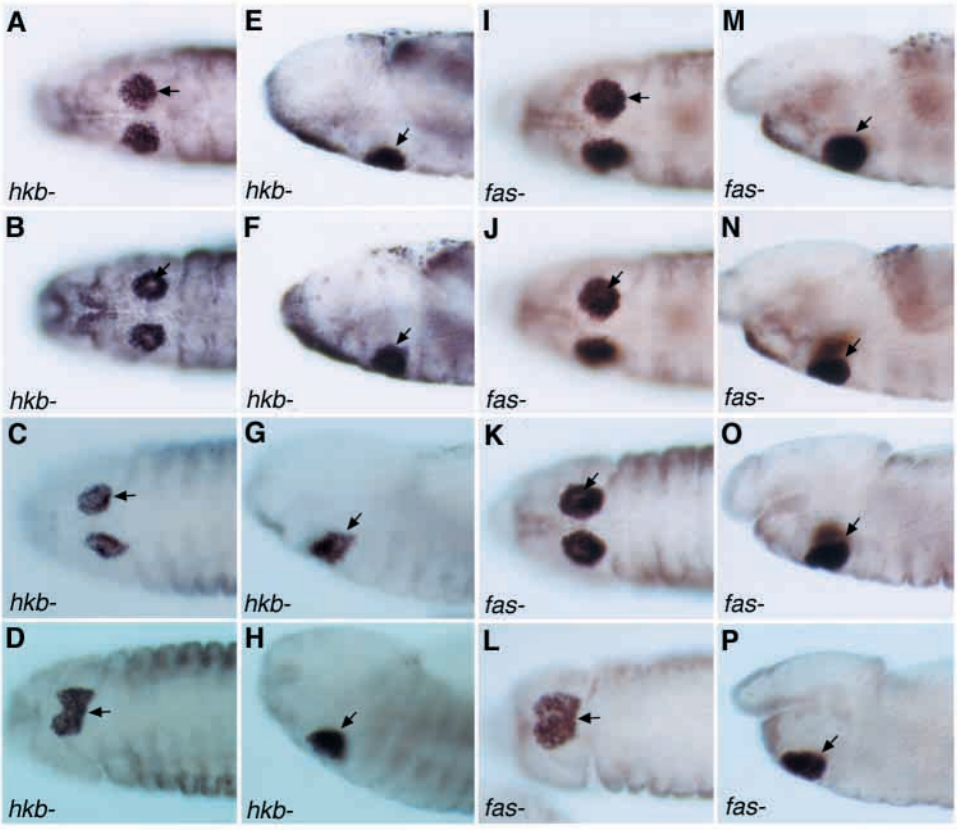

Fig. 5. Salivary gland tube formation is abnormal in *hkb* and *fas* mutant embryos. (A-H) *hkb* mutant embryos, (I-P) *fas* mutant embryos stained with α-dCREB-A. (A-D, I-L) Ventral views; (E-H, M-P) the corresponding lateral views. Embryos in (A,E,B,F,I,M,J,N) are at embryonic stage 11, while embryos in (C,G,K,O) are at embryonic stage 12 and embryos in (D,H,L,P) are at embryonic stage 13. The salivary gland placodes of *hkb* and *fas* mutant embryos appear morphologically normal (A,E,I,M, arrows). Both *hkb* (B,F, arrows) and *fas* (J,N, arrows) mutant embryos begin invagination in the center of the placode. The invaginating salivary glands of *hkb* mutant embryos are trapezoidal shaped (C,G, arrows). The invaginating pit of *fas* mutant embryos is trough-shaped and is located near the center of the placode (K,O, arrows). The salivary glands of *hkb* and *fas* mutant embryos fuse at the midline and are dome-shaped (D,H,L,P, arrows). The data represented here and in the subsequent figure were acquired for hkb^{A231R1} and fas^{2} embryos. Identical phenotypes were observed for hkb^{2} and fas^{1} embryos.

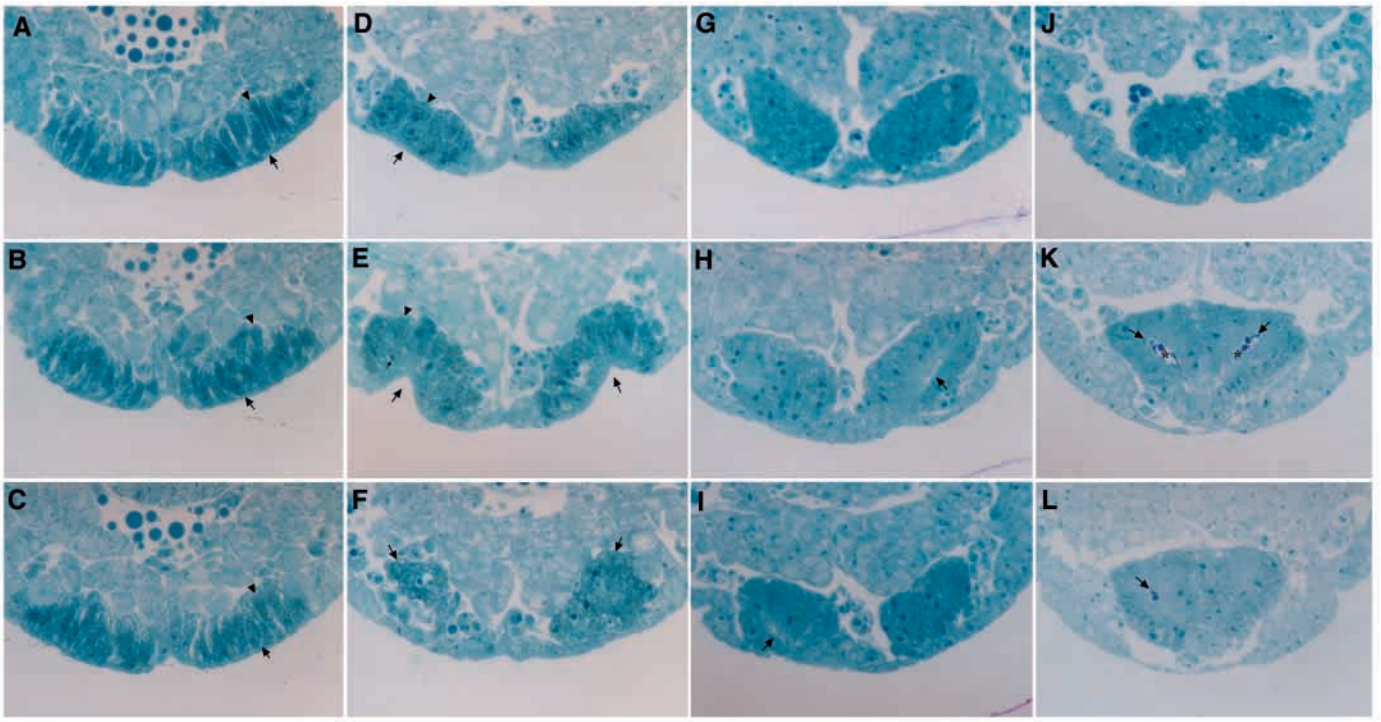

Fig. 6. Histological analysis of salivary gland invagination in *hkb* mutant embryos. The three panels of each column are cross sections from the anterior (A,D,G,J), medial (B,E,H,K) and posterior (C,F,I,L) regions of the same placode. Cells throughout the salivary gland placode are elongated with nuclei in apical (A-C, arrows) and basal (A-C, arrowheads) positions. The invaginating pit is wide and includes most of the cells along the width of the placode (E, arrows). The nuclei of some cells are located basally (E, arrowheads), while those in others are located apically (E, small arrows). Cells in the anterior part of the placode have nuclei in apical (D, arrow) and basal positions (D, arrowhead). Cells posterior to the invaginating pit have been internalized (F, arrows). Cells of the internalized salivary glands are arranged as a monolayer surrounding a central lumen (G-I, arrows). The internalized salivary glands fuse to form a dome-shaped organ with a common lumen (I,K asterisks, L) in which possible secretory products stained darkly for Methylene Blue are observed (K,L, arrows). A minimum of three embryos at each stage of invagination was analyzed. Although only three representative cross sections are shown, 1 μm thin sections of the entire salivary gland primordia at the indicated stages of invagination were acquired for analysis.

immuno-staining to detect β-gal in a viable *hkb* P-element insertion line, AI7-*hkb*, reveal a dynamic expression pattern in the salivary gland primordia (Fig. 4). At the stage when the salivary gland primordium is approximately square, *hkb* expression is first detected in a dorsal-posterior quadrant of approximately 4-5 rows of cells (Fig. 4A,E,I,K), correlating with the earliest expression of *trachealess* (Fig. 4I), dCREB-A (Fig. 4K) and *Sex combs reduced* (data not shown). Slightly later, when the salivary gland primordium becomes round-shaped, low levels of *hkb* expression are also observed in the dorsal-medial cells. *hkb* expression is excluded from the remaining cells of the placode at this stage (Fig. 4B,F,J). This pattern is soon followed by a second site of high level *hkb* expression in the dorsal-anterior cells of the placode (Fig. 4C,G,L). *hkb* expression levels in the ventral cells remain low (Fig. 4C,G,L). Just prior to internalization, low levels of *hkb* mRNA are observed in nearly all cells of the placode (Fig. 4D). *hkb* RNA is not detected once the dorsal-posterior cells have begun to internalize (data not shown). The continued presence of β-gal in the salivary gland during and after internalization (Fig. 4H and data not shown), when the RNA for *hkb* is no longer detected, is probably due to the stability of β-gal. HKB protein expression in the salivary gland placode could not be assessed with the currently available α-HKB antibodies (data not shown). This analysis demonstrates that the temporal expression of *hkb* in different regions of the placode presages the sequential wave of invagination that internalizes the secretory primordia (Fig. 4I,M). The dorsal-posterior cells are the first cells to express high levels of *hkb*, and are also the first cells to invaginate (Fig. 2). Cells immediately anterior to the dorsal-posterior cells are the next group of cells to express *hkb* and are also the next to invaginate. The subsequent second site of high level *hkb* expression in the anteriormost region of the placode correlates with the cell shape changes observed in the anteriormost cells (Fig. 2E,J). Finally, low *hkb* levels are detected in almost all cells of the primordia just prior to the initiation of invagination (Fig. 4D).

Internalization and salivary gland shape are altered in *hkb* mutant embryos

The dynamic pattern of *hkb* expression in the salivary gland placode suggested a possible role for *hkb* in directing internalization. Thus, we examined salivary glands in *hkb* mutants with the same techniques used to analyze WT embryos. By whole-mount analysis, the salivary gland placodes of *hkb* mutants look identical to those of WT embryos; the cells stain with α-dCREB-A and reside at the ventral surface (Fig. 5A,E). The first defect observed at a gross morphological level is the incorrect positioning of the initial

site of internalization; the first cells to internalize in *hkb* mutant embryos are those in the middle of the placode (Fig. 5B,F). Later, the salivary glands in *hkb* mutant embryos are trapezoidal-shaped in both ventral and lateral views (Fig. 5C,G). Although all of the secretory cells are internalized in *hkb* mutants, they never form the characteristic cigar-shaped tubes of the WT salivary glands; instead *hkb* mutants form dome-shaped structures that eventually fuse along the ventral midline (Fig. 5D,H). Thus, in addition to an early defect in the localization of the salivary gland pit, *hkb* mutant embryos form salivary glands whose shape is dramatically aberrant.

The histological analysis of *hkb* mutant embryos supports the observations from the whole-mount analysis described above. When *hkb* mutant embryos are in stage I of salivary gland internalization, the placode cells look identical to WT placode cells; they are elongated with nuclei randomly positioned in the apical and basal domains (Fig. 6A-C). Later, the invaginated salivary gland pit of *hkb* mutant embryos is mislocated and is a mixture of wedge-shaped cells with constricted apices and basal nuclei, and elongated cells with randomly positioned nuclei (Fig. 6E). This arrangement of cell morphology in the *hkb* salivary gland pits is in contrast to that of WT embryos, where all cells that comprise the pit have approximately the same length, and are wedge-shaped with basal nuclei (Fig. 2H). The *hkb* pit is also wider and shallower than the WT salivary gland pits, and appears to include more cells. Although all secretory cells of *hkb* mutant embryos are eventually internalized, the salivary glands are positioned more anteriorly, and lie closer to the ventral midline and the body wall than the salivary glands of WT embryos (Fig. 6G-I). The two salivary glands of *hkb* mutant embryos then fuse at the ventral midline and form 'dome-shaped' organs with a common lumen (Fig. 6J-L). Dark Methylene Blue staining is detected in the lumen, which may correspond to salivary gland secretory products (Fig. 6K,L).

By SEM analysis, the surfaces of the salivary gland placodes of *hkb* mutant embryos appear morphologically identical to those of WT embryos (Fig. 3E). Differences become evident only when the invaginating pits form in the *hkb* mutants (Fig. 3F). SEM confirms that the pits are misplaced, occurring in the approximate center of the primordia rather than in the dorsal-posterior region, and they are wider relative to WT pits (Fig. 3G). The order of invagination in the *hkb* mutants is also disrupted; cells immediately surrounding the pits appear to change shape and invaginate simultaneously (Fig. 3G). Once invagination of the secretory cells is complete in *hkb* mutant embryos, open pits remain, as observed in WT embryos (Fig. 3H).

Internalization and salivary gland shape are also altered in *fas* mutant embryos

Salivary gland cells in embryos carrying a null allele of *faint sausage*, fas^{IIA}, were previously reported to not invaginate (Liu et al., 1999). Our examination of salivary gland morphogenesis in *fas* mutant embryos revealed that the cells invaginate but show gross morphological defects that are very similar to those of *hkb* mutant embryos. By whole-mount analysis of *fas* mutant embryos stained with α-dCREB-A, the placodes appear morphologically identical to placodes of WT and *hkb* mutant embryos (Fig. 5I,M). At the stage when the dorsal-posterior pit forms in WT embryos, we observe a slight indentation near the center of the placode of *fas* mutant embryos, suggestive of cell shape changes (Fig. 5J,N). Although the initial indentation occurs at slightly variable locations in different embryos of similar age, the pit observed in late-stage *fas* mutants is trough-shaped and uniformly located close to the center of the placode (Fig. 5K,O). At late stages of embryogenesis, the overall morphology of the salivary glands of *fas* mutants is similar to that of *hkb* mutants; the glands are dome-shaped, are fused at the ventral midline and remain close to the embryo surface (Fig. 5L,P).

Although the salivary gland placodes of *fas* mutants appear identical to those of WT embryos at a gross morphological level, histological sections reveal significantly altered cell morphology. Instead of the monolayer of uniformly elongated epithelial cells that is observed in sections of WT embryos, placode cells in *fas* mutants are found in multiple layers, and are variably elongated (Fig. 7A-C). At later stages, the pit that forms in *fas* mutants is not as deep or wide as the pits of WT or *hkb* mutant embryos (Fig. 7E). Cells at the center of the pit appear elongated with basally positioned nuclei; however, the surrounding cells in the pit are round and found in multiple layers. Cells in the anterior (Fig. 7D) and posterior (Fig. 7F) parts of the gland also form multi-layered placodes. The salivary glands of *fas* mutants are eventually internalized, despite gross abnormalities in cell shape (Fig. 7G-I). The internalized gland is comprised of a mixture of elongated and wedge-shaped cells (Fig. 7H). Cells in the anterior (Fig. 7G) and posterior (Fig. 7I) parts of the gland are multi-layered. After internalization, the *fas* mutant salivary glands fuse into one dome-shaped organ, which is located close to the ventral surface, like the glands of *hkb* mutant embryos (Fig. 7J-L). Unlike the salivary gland cells of WT and *hkb* mutants, salivary gland cells of *fas* mutant embryos are not in an epithelial monolayer and, instead, appear to have condensed into a single, multilayered organ with remnants of a potentially contiguous lumen. As in the *hkb* mutant embryos (Fig. 6K,L), potential secretory products, indicated by dark Methylene Blue staining, are found in the lumen of *fas* mutant embryos (Fig. 7J-L).

By SEM, the surface morphology of the salivary gland placodes of *fas* mutant embryos is similar to that of WT and *hkb* mutants (Fig. 3I). In *fas* mutant embryos, a small number of cells in the approximate middle of the placode are the first to change shape and form a pit (Fig. 3J). The pits are much narrower than the pits of WT or *hkb* mutants, averaging 2-3 μm in diameter compared to 5 and 10.5 μm in WT and *hkb* mutants, respectively (Fig. 3J,B,F). In contrast to *hkb* mutant embryos, there is some directed movement of cells into the invaginating pit of *fas* mutant embryos. When the pit is first visible, cells immediately anterior to it have narrow and round apices, indicative of cell shape changes (Fig. 3J), and correspondingly, at later stages, the pit lengthens anteriorly, becoming trough-shaped (Fig. 3K). Similarly, the apical surfaces of the cells anterior to the trough-like pit are round, indicating that these cells have changed shape and will soon invaginate, whereas the apical surfaces of cells dorsal and ventral to the pit remain flat and broad, in keeping with their later time of invagination. When internalization of the salivary gland cells is complete, the surface morphology of the salivary pits of *fas* mutants is similar to that of WT and *hkb* mutant embryos (Fig. 3L).

The effect of *hkb* on the localization and expression of *fas* in the salivary gland

Since *fas* and *hkb* mutant embryos have similar salivary gland phenotypes at a gross morphological level, and *hkb* encodes a transcription factor, we examined the expression of *fas* in both WT and *hkb* mutant embryos. Prior to invagination, *fas* RNA and protein are expressed in all secretory cells in WT embryos (Fig. 8A, and data not shown). At the start of invagination, *fas* RNA levels decrease to the levels observed in surrounding epithelial cells (Fig. 8B), and it is no longer detected in cells that have been internalized (data not shown). At this stage, higher levels of FAS protein are detectable in all secretory cells, including the invaginating dorsal-posterior cells, relative to surrounding non-salivary gland cells (Fig. 8C). FAS protein is detected in all secretory cells that have internalized (Fig. 8D-F), and this level is maintained throughout the remainder of embryogenesis (Fig. 8F and data not shown). FAS protein levels appear highest at the apical membrane, although different fixation procedures alter the relative levels of protein detected (data not shown).

The early expression of *fas* RNA and protein are unchanged in embryos mutant for *hkb* (data not shown). Later, when elevated levels of FAS protein are observed in the invaginating dorsal-posterior cells of WT embryos, such elevated levels are instead observed in cells at the center of the glands in *hkb* mutants, and these cells are the first to internalize (Fig. 8G,H). In the internalized secretory cells, the level of FAS appears equivalent in *hkb* mutants and WT embryos (Fig. 8I,F). Thus, *hkb* affects *fas* expression transiently and only indirectly, by specifying the order in which secretory cells are internalized.

DISCUSSION

Salivary glands internalize through a defined series of coordinated cell shape changes

Our findings on how the tubular shape of the *Drosophila* salivary gland is achieved provide a paradigm for how other organs in other organisms are shaped during embryogenesis. Numerous examples exist on the sequential order of cell shape changes during epithelial morphogenesis, and its possible role in shaping the final organ. During invagination of the posterior midgut primordium in *Drosophila* embryos, apical constrictions occur first in the cells immediately dorsal to the pole cell cluster, then spread further dorsally, and then laterally until they reach the cells on the ventral side of the posterior pole (Sweeton et al., 1991). Similarly, avian and mammalian neurulation involves a series of regulated, sequential cell shape changes that transform a flat neural plate into a keyhole-shaped neural groove (reviewed in Schoenwolf and Smith, 1990). This transformation is made possible by the formation of specific hinge-points, the median hinge point (MHP), which anchors the neural plate to the notochord, and two lateral hinge points (LHP), which anchor the neural plate to surrounding tissues. Cells of the MHP and LHPs are of various shapes, and it is the conversion between these cell shapes that provides the driving force for shaping the neural groove (Smith and Schoenwolf, 1988; Smith et al., 1994). During formation of the lens placode as well, invagination occurs more rapidly in the dorsal part of the placode (Hilfer, 1983). As a consequence, the lens pit is trough-shaped with the opening of the pit pointed ventrally. Despite these and other examples of regulated cell shape changes during organogenesis, the idea that the order in which cells change shape and internalize affects final morphology has not been previously tested. Our studies on WT, *hkb* and *fas* mutant embryos provide the first evidence for a critical role for the regulated, sequential order of cell shape changes in establishing the final shape of an organ.

The shape of the salivary glands of wild-type embryos at multiple stages of internalization correlates with the number and position of cells invaginating at any given time. Early, when invagination begins with the dorsal-posterior cells and begins to include more dorsal-anterior cells (Fig. 2E,H), we observe a small pit directed dorsally (Figs 1E,F and 3B). Slightly later, when internalization is occurring nearly simultaneously in dorsal-medial and dorsal-anterior cells (Fig. 2J,K), we observe a narrow distal tube, which corresponds to the small number of cells initially internalized, and a wider proximal tube, which corresponds to the larger number of cells that are internalized later (Figs 1F and 3C). As the anterior and ventral cells are internalized (Fig. 2N,O), the tube is directed more posteriorly and laterally (Fig. 1G,H). Once all of the cells have internalized, the salivary gland adopts its characteristic cigar shape.

When the order of cell invagination is disrupted, morphology of the salivary glands is severely affected, such as in *hkb* and *fas* mutant embryos (Figs 4-6). In these embryos, invagination is initiated in the center of the placode, instead of the dorsal-posterior region, and the subsequent order of cell internalization is altered. As a consequence, salivary glands from *hkb* and *fas* mutant embryos are abnormal at all stages of internalization, and form dome-shaped salivary glands instead of cigar-shaped tubes (Fig. 4D,H,L,P). These results demonstrate that early events in the salivary gland placode, such as where the first cell shape changes occur, dictate later outcomes in forming the salivary gland tube.

The order of internalization also determines which cells in the primordia occupy which position in the mature tube. This relationship could be important for limiting the expression and function of certain genes to only a subset of cells in the mature salivary gland. For example, *Semaphorin II* (*Sema II*), which encodes a member of a family of guidance molecules (for a review, see Spriggs, 1999), is expressed in only the dorsal-posterior cells of the placode, the first cells to internalize. These cells continue to express *Sema II*, and once internalization is complete, occupy the distal half of the salivary gland tube where *Sema II* may function in positioning the gland, possibly by mediating adhesion to surrounding tissues (K. Henderson and D. J. A., unpublished results).

A role for HKB in the temporal and spatial control of internalization

The correlation between *hkb* expression and the order in which cells invaginate make HKB an excellent candidate for determining when and where cell shape changes will occur. Since HKB is a transcription factor, it must coordinate cell shape changes indirectly, through the regulation of one or more effector molecules. One obvious candidate target gene is *fog*, which encodes a putative secreted signal that mediates coordinated cell shape changes in the invaginating mesoderm and posterior gut endoderm during *Drosophila* gastrulation (Costa et al., 1994). Indeed, *fog*'s expression in the salivary gland primordia is dynamic like *hkb*'s: *fog* is initially expressed

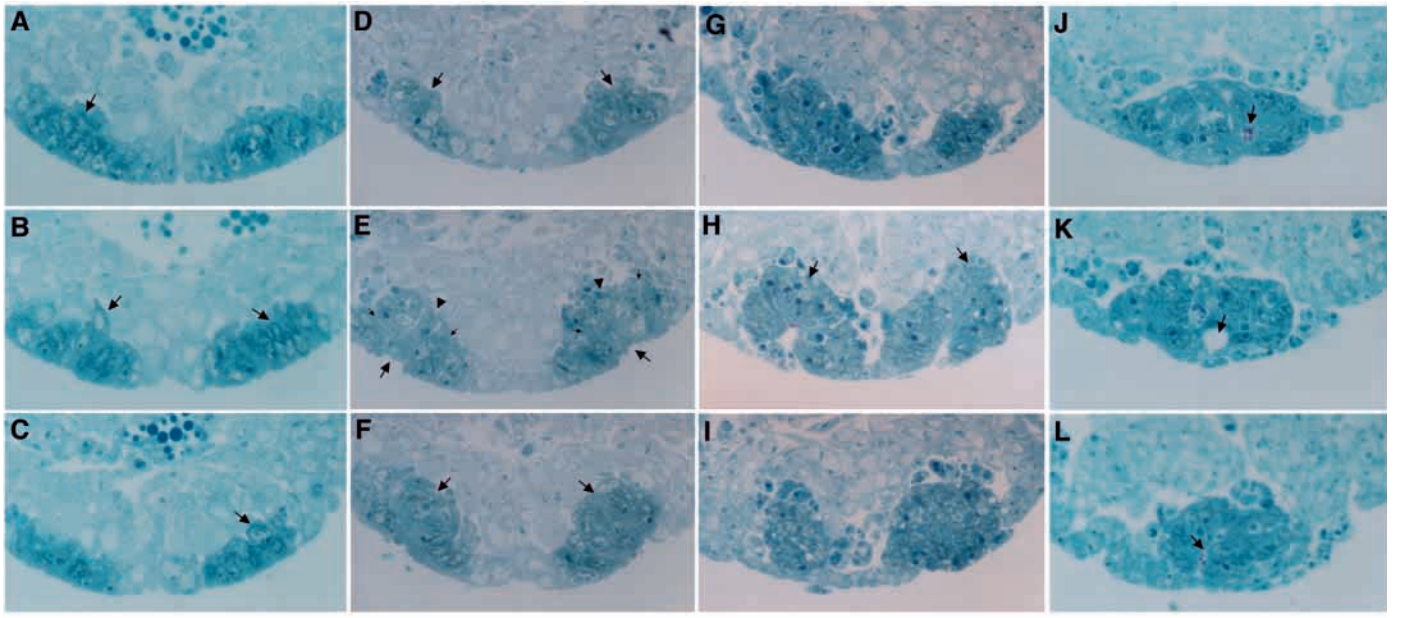

Fig. 7. Histological analysis of salivary gland invagination in *fa*s mutant embryos. The three panels of each column are cross sections from the anterior (A,D,G,J), medial (B,E,H,K) and posterior (C,F,I,L) regions of the same placode. Cells of the salivary gland placode are stacked upon each other in two or three rows (A-C, arrows). The invaginating pit is shallow (E, large arrows), and consists of one or two cells at the center that are elongated with basal nuclei (E, arrowheads), but the remaining cells of the pit are stacked upon each other (E, small arrows). Cells in the anterior (D, arrows), and posterior (F, arrows) parts of the gland are also found in multiple layers. All placode cells are internalized (G,H arrows, I). The fused salivary glands remain close to the ventral surface (J-L). The cells appear compacted, and lumina with methylene-blue stained secretory products are present (J-L, arrows). A minimum of three embryos at each stage of invagination was analyzed. Although only three representative cross sections are shown, 1 μm thin sections of the entire salivary gland primordia at the indicated stages of invagination were acquired for analysis.

in a diffuse crescent in the dorsal region of the salivary gland placode, and in all cells of the placode once invagination starts (data not shown). But unlike *hkb* expression, *fog* RNA continues to be expressed in the secretory cells that have internalized (data not shown). In *hkb* mutant embryos, the number of cells expressing detectable levels of *fog* is decreased, and *fog* expression appears to be higher in the approximate center of the primordia (data not shown), suggesting that *fog* expression in the salivary gland is partially HKB-dependent. This is not surprising given that *fog* expression in the posterior gut endoderm is diminished in *hkb* mutant embryos and completely absent in embryos simultaneously mutant for *hkb* and *tailless*, which encodes another transcription factor (Costa et al., 1993, 1994). We have examined salivary glands of *fog* mutant embryos and, although the embryos have severely abnormal gross morphologies, salivary gland internalization is relatively normal (data not shown). This finding suggests that either *fog* has no role in the regulated internalization of the salivary glands or that *fog* function is redundant in this tissue. Other candidate effector molecules have not yet been identified or tested. Our finding that salivary gland internalization is *fog*-independent, unlike the internalization of the mesodermal and endodermal primordia, suggests that different molecules signal cell shape changes in different tissues.

FAS maintains integrity of epithelial layer

While *hkb*'s expression pattern and mutant phenotype demonstrate a role in instructing the sequential order of invagination, the role of *fas* in salivary gland invagination is uncertain. The earliest defect detected in *fas* mutant embryos is the disorganization of the epithelium. However, FAS protein levels are barely above that of the surrounding epithelia at this stage. It is only during late invagination, and once invagination is complete, that elevated levels of FAS are observed in the salivary glands. Therefore, the altered shape of *fas* salivary glands could be due either to *fas'* early role in maintaining the integrity of the epithelium, or to its possible role in late stages of invagination, or both. In two other systems, *fas* has been shown to play a role in tissue organization. In the absence of *fas* function, the epidermis and CNS are disorganized, and the ventral nerve cord does not condense completely. As a consequence, neurons are not properly relocated and their axonal migrations are abnormal (Lekven et al., 1998). In the developing heart tube, *fas* is required both for the proper alignment of ipsilateral cardioblasts during their dorsal migration and for determining the correct number of cardioblasts (Haag et al., 1999). We believe that *fas* plays a similar role in organization of the salivary epithelium. In *fas* mutant embryos where the salivary placode is a multi-layered epithelia, secreted signaling molecules, presumably regulated by HKB, may not be able to travel the distance required to act effectively. Alternatively, FAS may have a more direct role in the reception or transmission of signals that lead to salivary gland invagination.

Internalization in the absence of instructive signals

In *hkb* mutant embryos, salivary gland primordial cells undergo the characteristic cell shape changes and invaginate, albeit in a different region of the placode. This phenotype suggests that

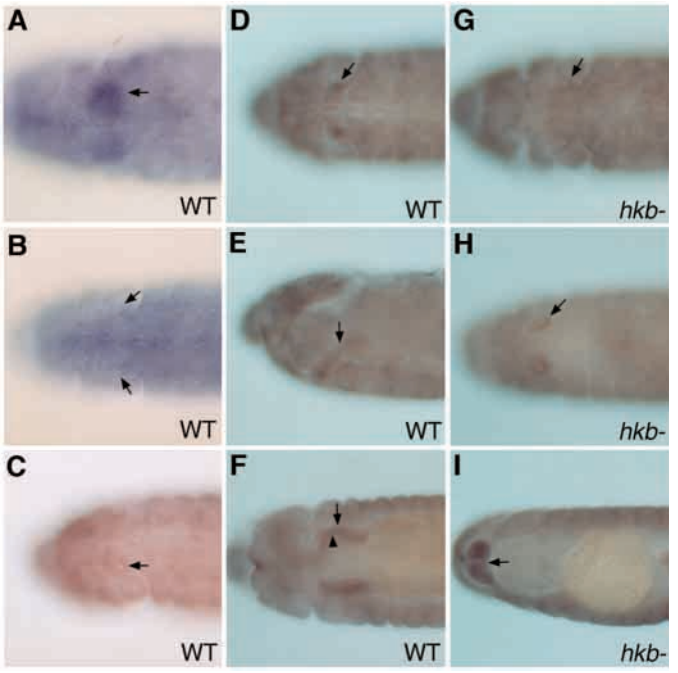

Fig. 8. Localization of *fas* RNA and protein in WT and *hkb* mutant embryos. (A,B) Whole-mount in situ hybridizations of WT embryos with an antisense *fas* RNA probe. (C-F) WT embryos stained with α-FAS. (G-I) *hkb* mutant embryos stained with α-FAS. *fas* RNA is detected in the salivary gland placodes (A, arrow). When invagination begins, levels of *fas* RNA in the secretory primordia is equivalent to that of surrounding, non-salivary cells (B, arrows). FAS protein is expressed at low levels in the salivary gland placode at the time of invagination (C, arrow). As invagination progresses, FAS protein is expressed at higher levels in the invaginating cells (D, arrow), and cells that have been internalized (E, arrows). (E) Lateral view of the same embryo in D. Once internalization is complete, FAS is expressed in all cells of the salivary gland tube (F, arrow) and is slightly enriched near the lumenal surface (F, arrowhead). FAS is expressed in *hkb* mutant embryos in the early (G, arrow) and the late invaginating pit (H, arrow), and when the internalized salivary glands have fused (I, arrow).

in the absence of HKB acting as an instructive signal, cells may activate a default mechanism for invagination. We propose three possible methods by which salivary gland cells can be internalized in the absence of *hkb*. First, invagination of the central cells in the salivary gland placode of *hkb* and *fas* mutant embryos could be due to an as yet unidentified molecule whose expression is independent of *hkb*, and which mediates cell shape change in only these central cells. Such a molecule would only be active in the absence of *hkb* function, leading to the invagination of the central cells first. *fork head* (*fkh*) encodes a transcription factor whose early expression in the salivary gland placodes is HKB-independent. The salivary glands are not internalized in *fkh* mutant embryos although the first cell shape changes are initiated at the right position in the primordia (M. M. Myat and D. J. Andrew, unpublished observations). This phenotype suggests that FKH may normally fuel internalization, perhaps providing sufficient force to direct internalization at an ectopic site in the absence of *hkb* function.

In the second model, cells could invaginate without instructive signals to relieve the stress and tension at the embryo surface. Odell and colleagues (1981) have constructed a mathematical model to explain how apical constriction of one cell could propagate a wave of constrictions leading to invagination of the entire epithelium. They propose that if the contractile microfilament network beneath the apical surface membrane stretches beyond a threshold point, the contractile system ‘fires’, triggering contraction of the apical surface membrane. They further propose that contraction of the first trigger cell could initiate a wave of contractions as each cell stretches the apical surface membrane of neighboring cells, causing them to fire, and contract in turn. The role of surface tension in selecting the site of cell shape change is supported by experiments where *fog* was expressed throughout the early *Drosophila* embryo (Morize et al., 1998). This ectopic *fog* expression resulted in the apical flattening without constriction of all cells in the embryo, possibly due to uniform tension at the embryo surface. Apical constrictions occurred only in cells adjacent to dividing cells, indicating that the rounding up of cells during mitosis releases the tension at the surface of the embryos, and allows those cells located next to mitotically active cells to constrict their apices. It is possible that the center of the placode is the site of the greatest surface tension. In the absence of a chemical signaling event that would normally cause the dorsal-posterior cells to constrict apically, cells in the center of the placode may fire by default to relieve the surface tension imposed by the stretching of the apical surface membrane. This would explain why the central cells of *hkb* mutant embryos are the first to invaginate, and would also explain the aberrant internalization observed in *fas* mutant embryos. The invaginating pit of *fas* mutant embryos consists of only one or two cells at the center of the pit that are elongated and wedge-shaped. The cells in the dorsal and ventral parts of the pit are not only multi-layered, but are round or variably elongated. The contraction of the one or two central cells in *fa*s mutant embryos may be sufficient to form a shallow pit, allowing the surrounding cells to move into the interior, without themselves going through the characteristic cell shape changes.

In our third model, internalization of salivary glands in *hkb* and *fas* mutant embryos may occur by an altogether different mechanism. An exception to the apical constriction and nuclear migration mode of invagination occurs during sea urchin gastrulation, where active secretion at the apical surface of the epithelia is proposed to create a complex, bilayered extracellular matrix (ECM). The layer of ECM closest to the epithelial cells swells relative to the outer layer due to active secretion. Since the outer layer does not swell, hydration of the inner layer bends the ECM and attached epithelium inwards, driving internalization (Lane et al., 1993). This bending bilayer model would explain why salivary gland internalization begins in the approximate center of the primordia in both the *hkb* and *fas* mutant embryos.

Studies of the *Drosophila* salivary gland are likely to be instructive and will provide a basis for understanding the genetic control of epithelial morphogenesis in higher organisms. Although we are clearly at an early stage in understanding the details of salivary gland formation, our studies have revealed the importance of early events in determining the final, overall shape of an organ. The identification of molecules such as *hkb* and *fas* provide

essential tools for learning how these early events are mediated. Instructive signals initiated by molecules such as HKB determine the order in which cell shape changes occur. However, for these signals to be properly received and interpreted, the integrity of the epithelial cells must be maintained by molecules such as FAS. To gain a better understanding of how these events are coordinated at the molecular and cellular level, we have initiated a mutagenesis screen to identify genes involved in these early aspects of salivary gland tube formation.

We thank E. Abrams, who first brought to our attention the salivary gland defects in late *hkb* mutant embryos. We thank V. Hartenstein for the FAS antisera. We thank the *Drosophila* Stock Center and C. Doe for the *fas* and *hkb* fly stocks, and E. Wieschaus for the *fog* fly stock. We thank the C. Goodman Laboratory for the *hkb* P-element insertion line. We are grateful to M. Delannoy and C. Cooke for teaching the essentials of electron microscopy to M. M. M. Information regarding *fas* and *hkb* cDNAs was provided by the Berkeley *Drosophila* Genome Project. We thank P. Bradley, A. Haberman, K. Henderson, A. Hubbard, C. Machado, and P. Wilson for the critical reading of our manuscript. We thank K. Patel for excellent technical assistance. Finally, we thank all of the members of the Andrew laboratory for their patience and more general intellectual and material contributions to this work. This work was supported by an NIH grant to D. J. A. (# RO1 GM 51311) and a Jane Coffin Childs postdoctoral fellowship to M. M. M.

REFERENCES

Alvarez, I. S. and Navascues, J. (1990). Shaping, invagination, and closure of the chick embryo otic vesicle: scanning electron microscopic and quantitative study. *Anat. Rec.* **228**, 315-326.

Andrew, D. J., Baig, A., Bhanot, P., Smolik, S. M. and Henderson, K. D. (1997). The *Drosophila dCREB-A* gene is required for dorsal/ventral patterning of the larval cuticle. *Development* **124**, 181-193.

Andrew, D. J., Henderson, K. D. and Seshaiah, P. (2000). Salivary gland development in Drosophila melanogaster. *Mech. Dev.* In press.

Barrett, K., Leptin, M. and Settleman, J. (1997). The Rho GTPase and a putative RhoGEF mediate a signaling pathway for the cell shape changes in *Drosophila* gastrulation. *Cell* **91**, 905-915.

Bowes, R. C., 3rd, Lightfoot, R. T., Van De Water, B. and Stevens, J. L. (1999). Hepatocyte growth factor induces tubulogenesis of primary renal proximal tubular epithelial cells. *J. Cell Physiol.* **180**, 81-90.

Brönner, G., Chu-LaGraff, Q., Doe, C. Q., Cohen, B., Weiogel, D., Taubert, H. and Jäckle, H. (1994). Spi/egr-like zinc-finger protein required for endoderm specification and germ-layer formation in *Drosophila*. *Nature* **369**, 664-668.

Campos-Ortega, J. A. and Hartenstein, V. (1997). *The Embryonic Development of* Drosophila melanogaster. Berlin Heidelberg: Springer-Verlag.

Costa, M., Sweeton, D., and Wieschaus, E. (1993). Gastrulation in *Drosophila*: cellular mechanisms of morphogenetic movements. In *Development of* Drosophila melanogaster (ed. M. Bate and A. Martinez-Arias), pp. 425-465. Cold Spring Harbor, New York: Cold Spring Harbor Laboratory Press.

Costa, M., Wilson, E. T. and Wieschaus, E. (1994). A putative cell signal encoded by the folded gastrulation gene coordinates cell shape changes during *Drosophila* gastrulation. *Cell* **76**, 1075-89.

Davies, J. A. and Bard, J. B. (1998). The development of the kidney. *Curr. Top. Dev. Biol.* **39**, 245-301.

Ettensohn, C. A. (1985). Mechanisms of epithelial invagination. *Q. Rev. Biol.* **60**, 289-307.

Flybase (1999). The FlyBase database of the *Drosophila* Genome Projects and community literature. The FlyBase Consortium. *Nucleic Acids Res*. **27**, 85-88.

Glaser, O. R. (1916). The theory of autonomous folding in embryogenesis. *Science* **44**, 505-509.

Glazer, L. and Shilo, B.-Z. (1991). The *Drosophila* FGF-R homolog is expressed in the embryonic tracheal system and appears to be required for directed tracheal cell extension. *Genes Dev.* **5**, 697-705.

Gudernatsch, J. F. (1913). Concerning the mechanism and direction of embryonic folding. *Anat. Rec.* **7**, 411-431.

Gumbiner, B. M. (1992). Epithelial morphogenesis. *Cell* **69**, 385-387.

Haag, T. A., Haag, N. P., Lekven, A. C. and Hartenstein, V. (1999). The role of cell adhesion molecules in *Drosophila* heart morphogenesis: *faint sausage*, *shotgun/DE-cadherin*, and *laminin A* are required for discrete stages in heart development. *Dev. Biol.* **208**, 56-69.

Hacker, U., Lin, X. and Perrimon, N. (1997). The *Drosophila* sugarless gene modulates Wingless signaling and encodes an enzyme involved in polysaccharide biosynthesis. *Development* **124**, 3565-3573.

Hacker, U. and Perrimon, N. (1998). DRhoGEF2 encodes a member of the Dbl family of oncogenes and controls cell shape changes during gastrulation in Drosophila. *Genes Dev.* **12**, 274-284.

Hardin, J. and Keller, R. (1988). The behaviour and function of bottle cells during gastrulation of *Xenopus laevis*. *Development* **103**, 211-30.

Hilfer, S. R. (1983). Development of the eye of the chick embryo. *Scan Elect. Microsc* **3**, 1353-1369.

Hogan, B. L. and Yingling, J. M. (1998). Epithelial/mesenchymal interactions and branching morphogenesis of the lung. *Curr. Opin. Genet. Dev.* **8**, 481-6.

Isaac, D. D. and Andrew, D. J. (1996). Tubulogenesis in *Drosophila*: a requirement for the *trachealess* gene product. *Genes Dev.* **10**, 103-117.

Kjelsberg, C., Sakurai, H., Spokes, K., Birchmeier, C., Drummond, I., Nigam, S. and Cantley, L. G. (1997). Met –/– kidneys express epithelial cells that chemotax and form tubules in response to EGF receptor ligands. *Am. J. Physiol.* **272**, F222-228.

Lane, M. C., Koehl, M. A., Wilt, F. and Keller, R. (1993). A role for regulated secretion of apical extracellular matrix during epithelial invagination in the sea urchin. *Development* **117**, 1049-60.

Lehmann, R. and Tautz, D. (1994). *In situ* Hybridization to RNA. In Drosophila melanogaster: *Practical Uses in Cell and Molecular Biology* (ed. L. S. B. Goldstein and E. A. Fyrberg), pp. 575-598. San Diego, Academic Press.

Lekven, A. C., Tepass, U., Keshmeshian, M. and Hartenstein, V. (1998). *faint sausage* encodes a novel extracellular protein of the immunoglobulin superfamily required for cell migration and the establishment of normal axonal pathways in the *Drosophila* nervous system. *Development* **125**, 2747-2758.

Leptin, M. (1999). Gastrulation in *Drosophila*: the logic and the cellular mechanisms. *EMBO J.* **18**, 3187-92.

Leptin, M. and Grunewald, B. (1990). Cell shape changes during gastrulation in *Drosophila*. *Development* **110**, 73-84.

Liu, X., Kiss, I. and Lengyel, J. A. (1999). Identification of genes controlling malpighian tubule and other epithelial morphogenesis in *Drosophila melanogaster*. *Genetics* **151**, 685-695.

Llimargas, M. and Casanova, J. (1999). EGF signalling regulates cell invagination as well as cell migration during formation of tracheal system in *Drosophila*. *Dev. Genes Evol.* **209**, 174-179.

Metzger, R. J. and Krasnow, M. A. (1999). Genetic control of branching morphogenesis. *Science* **284**, 1635-1639.

Minot, C. S. (1903). *A Laboratory Textbook of Embryology*. Philadelphia: P. Blakiston's Son and Co.

Montesano, R., Matsumoto, K., Nakamura, T. and Orci, L. (1991a). Identification of a fibroblast-derived epithelial morphogen as hepatocyte growth factor. *Cell* **67**, 901-908.

Montesano, R., Schaller, G. and Orci, L. (1991b). Induction of epithelial tubular morphogenesis in vitro by fibroblast-derived soluble factors. *Cell* **66**, 697-711.

Morize, P., Christiansen, A. E., Costa, M., Parks, S. and Wieschaus, E. (1998). Hyperactivation of the folded gastrulation pathway induces specific cell shape changes. *Development* **125**, 589-97.

Odell, G. M., Oster, G., Alberch, P. and Burnside, B. (1981). The mechanical basis of morphogenesis. I. Epithelial folding and invagination. *Dev. Biol.* **85**, 446-62.

Parks, S. and Wieschaus, E. (1991). The *Drosophila* gastrulation gene *concertina* encodes a Gα-like protein. *Cell* **64**, 447-458.

Reuter, R., Panganiban, G. E. F., Hoffmann, F. M. and Scott, M. P. (1990). Homeotic genes regulate the spatial expression of putative growth factors in the visceral mesoderm of *Drosophila* embryos. *Development* **110**, 1031-1040.

Ridley, A. J. (1995). Rho-related proteins: actin cytoskeleton and cell cycle. *Curr. Opin. Genet. Dev.* **5**, 24-30.

Sakurai, H. and Nigam, S. K. (1997). Transforming growth factor-beta selectively inhibits branching morphogenesis but not tubulogenesis. *Am. J. Physiol.* **272**, F139-146.

Sakurai, H., Tsukamoto, T., Kjelsberg, C. A., Cantley, L. G. and Nigam, S. K. (1997). EGF receptor ligands are a large fraction of in vitro branching morphogens secreted by embryonic kidney. *Am. J. Physiol.* **273**, F463-472.

Sakurai, Y., Sawada, T., Chung, Y. S., Funae, Y. and Sowa, M. (1997). Identification and characterization of motility stimulating factor secreted from pancreatic cancer cells: role in tumor invasion and metastasis. *Clin. Exp. Metastasis* **15**, 307-317.

Schoenwolf, G. C. and Smith, J. L. (1990). Mechanisms of neurulation: traditional viewpoint and recent advances. *Development* **109**, 243-70.

Smith, J. L. and Schoenwolf, G. C. (1988). Role of cell-cycle in regulating neuroepithelial cell shape during bending of the chick neural plate. *Cell Tissue Res.* **252**, 491-500.

Smith, J. L., Schoenwolf, G. C. and Quan, J. (1994). Quantitative analyses of neuroepithelial cell shapes during bending of the mouse neural plate. *J. Comp. Neurol.* **342**, 144-51.

Smolik, S. M., Rose, R. E. and Goodman, R. H. (1992). A cyclic AMP-responsive element-binding transcriptional activator in *Drosophila* melanogaster, dCREB-A, is a member of the leucine zipper family. *Mol. Cell Biol.* **12**, 4123-4131.

Spriggs, M. K. (1999). Shared resources between the neural and immune systems: semaphorins join the ranks. *Curr. Opin. Immunol.* **11**, 387-91.

Sutherland, D. C., Samakovlis, C. and Krasnow, M. A. (1996). *branchless* encodes a *Drosophila* FGF homolog that controls tracheal cell migration and the pattern of branching. *Cell* **87**, 1091-1101.

Sweeton, D., Parks, S., Costa, M. and Wieschaus, E. (1991). Gastrulation in *Drosophila*: the formation of the ventral furrow and posterior midgut invaginations. *Development* **112**, 775-89.

Vainio, S. and Muller, U. (1997). Inductive tissue interactions, cell signaling, and the control of kidney organogenesis. *Cell* **90**, 975-978.

Vincent, S., Ruberte, E., Grieder, N. C., Chen, C. K., Haerry, T., Schuh, R. and Affolter, M. (1997). DPP controls tracheal cell migration along the dorsoventral body axis of the *Drosophila* embryo. *Development* **124**, 2741-50.

Wappner, P., Gabay, L. and Shilo, B.-Z. (1997). Interactions between the EGF receptor and DPP pathways establish distinct cell fates in the tracheal placodes. *Development* **124**, 4707-4716.

Wilk, R., Weizman, I. and Shilo, B.-Z. (1996). *trachealess* encodes a bHLH-PAS protein that is an inducer of tracheal cell fates in *Drosophila*. *Genes Dev.* **10**, 93-102.

Woolf, A. S., Kolatsi-Joannou, M., Hardman, P., Andermarcher, E., Moorby, C., Fine, L. G., Jat, P. S., Nobel, M. D. and Gherardi, E. (1995). Roles of hepatocyte growth factor/scatter factor and the met receptor in the early development of the metanephros. *J. Cell Biol.* **128**, 171-184.